SDS-22 stabilizes the PP1 catalytic subunits GSP-1/-2 contributing to polarity establishment in *C. elegans* embryos

Yi Li[1], Ida Calvi[2], Monica Gotta[1*]

[1] Department of Cell Physiology and Metabolism, Faculty of Medicine, University of Geneva, Geneva 1211, Switzerland

[2] Friedrich Miescher Institute for Biomedical Research (FMI), Basel, Switzerland

*Correspondence: monica.gotta@unige.ch

Abstract

In many cells, cell polarity depends on the asymmetric distribution of the conserved PAR proteins, maintained by a balanced activity between kinases and phosphatases. The *C. elegans* one-cell embryo is polarized along the anterior-posterior axis, with the atypical protein kinase C PKC-3 enriched in the anterior, and the ring finger protein PAR-2 in the posterior. PAR-2 localization is regulated by PKC-3 and the PP1 phosphatases GSP-1/-2. Here, we find that, similar to GSP-2 depletion, depletion of the conserved PP1 interactor SDS-22 results in a partial rescue of the polarity defects of a *pkc-3* temperature-sensitive mutant. Consistent with the rescue, SDS-22 depletion or mutation results in reduced GSP-1/-2 protein levels and activity. The decreased levels of GSP-1/-2 can be rescued by reducing proteasomal activity. Our data suggest that SDS-22 contributes to polarity by protecting the GSP-1 and GSP-2 catalytic subunits from proteasome-mediated degradation, supporting recent data in human cells showing the SDS22 is required to stabilize nascent PP1.

Introduction

Cell polarity is crucial for cellular and tissue architecture and function. In epithelial cells, polarity specifies the apical, basal and lateral membrane domains, enabling the selective barrier function of the epithelium (Riga *et al*, 2020). In migrating cells, front-to-rear polarity is crucial for cells to respond to environmental cues such as inflammatory factors, bacterial products, or growth factors (Llense & Etienne-Manneville, 2015). Cell polarity is crucial for asymmetric cell division, which is a prerequisite for stem cells to self-renew and to generate specialized daughter cells (Santoro *et al*, 2016) and for embryos to properly develop (Campanale *et al*, 2017). In many cells, polarity is regulated by the conserved partitioning defective (PAR) proteins, which were first identified in *C. elegans* (Goldstein & Macara, 2007; Lang & Munro, 2017).

The one-cell *C. elegans* embryo is polarized along the anterior-posterior axis. The anterior PAR proteins (the PDZ proteins PAR-3 and PAR-6, the atypical protein kinase C PKC-3 and the small GTPases CDC-42) are localized to the anterior cortex and cytoplasm of the embryo, while the posterior PAR proteins (the kinase PAR-1, the ring finger protein PAR-2, the lethal giant larvae ortholog LGL-1 and the CDC-42 GAP CHIN-1) are enriched in the posterior half of the embryo (reviewed in (Goehring, 2014; Lang & Munro, 2017)). Before polarity establishment, the anterior PAR proteins are uniformly localized on the cortex, while the posterior PAR proteins are localized in the cytoplasm. Shortly after fertilization, the centrosomal mitotic kinase Aurora A (AIR-1) removes the Rho GEF ECT-2 from the posterior pole (Kapoor & Kotak, 2019; Klinkert *et al*, 2019; Longhini & Glotzer, 2022; Zhao *et al*, 2019). This event initiates a cortical flow that segregates the anterior PAR proteins to the anterior and liberates the posterior cortex of the embryo, which is then occupied by the posterior PAR proteins (Munro *et al*, 2004).

Several studies have emphasized the importance of the regulation of PAR-2 phosphorylation by PKC-3 in establishing and maintaining cortical polarity (Hao *et al*, 2006; Motegi *et al*, 2011). Recently, our group has shown that PP1 phosphatases are also required for cortical polarity in one-cell embryos (Calvi *et al*, 2022). Before polarity establishment, PKC-3 phosphorylates PAR-2 and inhibits PAR-2 localization at the cortex (Hao *et al.*, 2006; Motegi *et al.*, 2011). The PP1 phosphatases GSP-1/-2 dephosphorylate PAR-2 allowing its cortical posterior accumulation and embryo polarization. Phosphomimetic mutants of PAR-2 (Hao *et al.*, 2006), or mutations that abolish the interaction between PAR-2 and GSP-1/-2 (Calvi *et al.*, 2022), prevent PAR-2 localization at the posterior, indicating that PP1 phosphatases are crucial for polarity establishment in *C. elegans* embryos.

Analogous to the intricate regulation of protein kinases, the activity of phosphatases towards specific substrates must be tightly regulated for proper cellular function, including cell division, heat shock

response, and glycogen metabolism (Ceulemans & Bollen, 2004). The activity of PP1 is primarily regulated post-translationally through interactions with PP1 interacting proteins, which guide its localization, substrate specificity and function. Over 200 PP1 interactors have been reported in different species and they regulate both in time and space the targeting of catalytic subunits towards different substrates (Aggen *et al*, 2000; Verbinnen *et al*, 2017; Virshup & Shenolikar, 2009). One non-canonical regulator of PP1 is the conserved SDS22 protein. In mammalian cells SDS22 suppresses Aurora B activity to control cell division (Duan *et al*, 2016; Posch *et al*, 2010; Wurzenberger *et al*, 2012). In *Drosophila melanogaster*, kinetochore-localized PP1–Sds22 dephosphorylates moesin at cell poles, facilitating anaphase elongation through polar relaxation (Rodrigues *et al*, 2015). PP1-87B and Sds22 also counteract aPKC and Aurora A kinase phosphorylation of Lgl, regulating apical-basal polarity in follicle epithelial cells (Moreira *et al*, 2019). In *Saccharomyces cerevisiae*, Sds22, along with Ypi1, is critical for the nuclear import and stabilization of PP1-Glc7 (Cheng & Chen, 2015; Peggie *et al*, 2002). Depletion of either Sds22 or Ypi1 results in mitotic arrest (Pedelini *et al*, 2007). Recent biochemical studies (Kueck *et al*, 2024) and studies in human cells (Cao *et al*, 2024) have demonstrated that SDS22 stabilizes nascent PP1 but needs to be removed from PP1 for the enzyme to be active. These two recent findings suggest that while SDS-22 is required for the biogenesis of PP1 holoenzymes, its removal is essential to have an active PP1. This dual role of SDS-22 explains how SDS22 behaves as an inhibitor in biochemical assays in vitro but as an activator in vivo (Cao *et al.*, 2024; Cao *et al*, 2022; Kueck *et al.*, 2024; Lesage *et al*, 2007).

In *C. elegans* GSP-1 and GSP-2, orthologues of human PP1β and PP1α, contribute to diverse processes such as germline immortality (Billmyre *et al*, 2019), sister chromatid cohesion in meiosis (Hsu *et al*, 2000; Tzur *et al*, 2012), centriole duplication (Peel *et al*, 2017), PAR-2 localization (Calvi *et al.*, 2022) in the early embryos, and the maintenance of epidermal junctions in adult worms (Beacham *et al*, 2022). Associated regulatory proteins have been identified for specific functions: for example, SDS-22 and SZY-2 modulate GSP-1 and GSP-2 activity in centriole duplication (Peel *et al.*, 2017), and APE-1 directs localization of GSP-2 to epidermal cell-cell junctions (Beacham *et al.*, 2022). However, the regulation of GSP-1 and GSP-2 during polarity establishment in one-cell embryos remains unknown.

Here we show that SDS-22 depletion partially rescues the polarity defects caused by reduced PAR-2 phosphorylation in the *pkc-3(ne4246)* mutant at the semi-restrictive temperature (24°C). Depletion of SDS-22 results in lower GSP-1 and GSP-2 protein levels which can be rescued by depleting proteasomal subunits. These results establish that SDS-22 contributes to cell polarity by regulating GSP-1/-2 levels and are consistent with and complement the recent data in mammalian cells showing that SDS22 is important to control the stability of the PP1 phosphatase (Cao *et al.*, 2024).

Result

Depletion of SDS-22 suppresses polarity defects of a temperature sensitive *pkc-3* mutant

We have previously found that PP1 phosphatases GSP-1 and GSP-2 counteract the activity of the atypical protein kinase PKC-3 and allow cortical localization of PAR-2 in *C. elegans* embryos. However, the regulator(s) of GSP-1 and GSP-2 in polarity establishment is not known. In immunoprecipitations followed by mass spectrometry analysis of mNG::GSP-2 from embryos, we identified three interactors that have been previously reported as evolutionarily conserved PP1 regulators: SDS-22, APE-1 and SYZ-2(I-2) (Fig EV1, Dataset EV1 and EV2).

When the temperature sensitive mutant *pkc-3(ne4246)* is grown at semi-permissive temperature, the residual PKC-3 activity is not sufficient to exclude PAR-2 from the anterior cortex. These embryos cannot establish polarity and die. Depletion of GSP-2 in this strain suppresses PAR-2 mislocalization and the resulting polarity defects, thereby rescuing embryonic lethality. We first asked whether depletion of any of these three identified regulators suppresses the embryonic lethality of *pkc-3(ne4246); gfp::par-2* embryos at the semi-permissive temperature of 24°C (temperature used in all experiments with the *pkc-3(ne4246)* mutant, unless otherwise stated), similar to depletion of GSP-2. None of these three regulators was able to suppress the embryonic lethality (Fig 1A). SDS-22 depletion alone resulted in 73.6% of embryonic lethality in the *gfp::par-2* strain, consistent with previous findings (Peel *et al.*, 2017). We then investigated if any of these regulators was able to rescue the aberrant PAR-2 localization of *pkc-3(ne4246)* embryos. Neither APE-1 nor SYZ-2 depletion rescued the symmetric PAR-2 localization observed in *pkc-3(ne4246); gfp::par-2* embryos (Fig EV2A). In contrast, depletion of SDS-22 resulted in PAR-2 localization being enriched in the posterior cortex in 87.5% of the one-cell stage embryos (Fig 1B,C) and PAR-2 was localized to the P1 blastomere after the first cell-division (Movie EV1). Depletion of SDS-22 in otherwise wildtype *gfp::par-2* embryos did not impair anterior-posterior polarity, with PAR-2 restricted to the posterior cortex (Fig 1D), indicating that the lethality caused by loss of SDS-22 is not the result of impaired PAR polarity establishment. However, similar to what has been observed in GSP-2 depleted embryos (Calvi *et al.*, 2022), the PAR-2 domain was smaller (Fig 1D, Fig EV2B). SDS-22 depleted embryos also displayed a smaller size (Fig EV2C).

We then investigated whether SDS-22 depletion, similar to GSP-2 depletion, rescued aberrant PAR-2 localization in another genetic background. When the PP1 binding motif in PAR-2 (164 RLFF 167) is optimized by a single amino acid substitution (L165V, resulting in RVFF, based on previous studies that show better binding to PP1(Meiselbach *et al*, 2006)), PAR-2 abnormally occupies the anterior cortex in early embryos. This phenotype is rescued by depletion of GSP-2, suggesting that it depends on higher activity of GSP-2 on PAR-2 (Calvi *et al.*, 2022). SDS-22 depletion also rescued the anterior PAR-2 domain observed in *gfp::par-2(L165V)* embryos as anterior PAR-2 was observed in only 45.5% of *gfp::par-2(L165V); sds-22(RNAi)* embryos compared to 100% *gfp::par-2(L165V); ctrl(RNAi)* embryos (Fig EV3).

Fig 1: SDS-22 depletion suppresses polarity defects of *pkc-3(ne4246)* mutant.

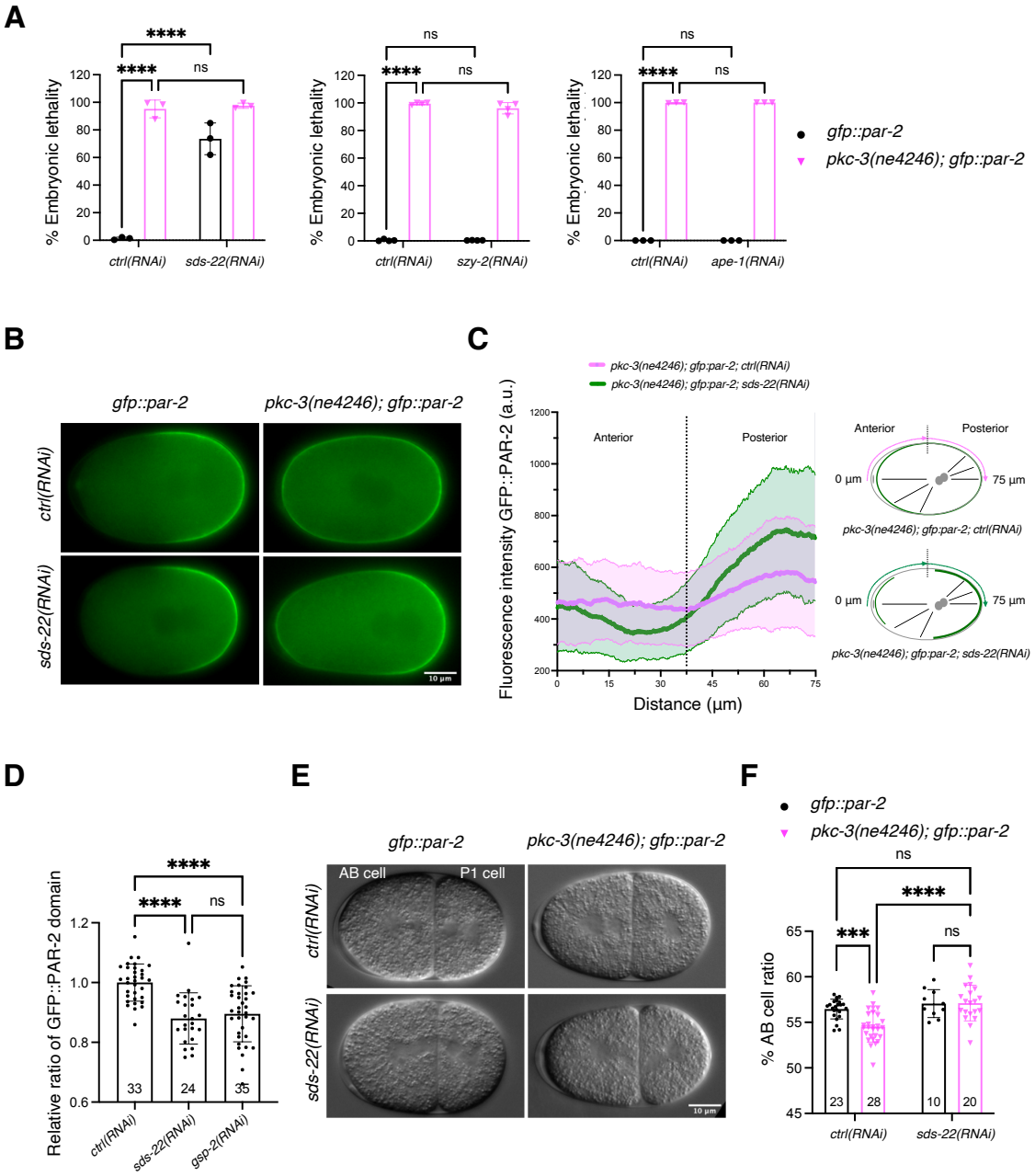

Fig 1: SDS-22 depletion partially suppresses the polarity defects of the *pkc-3(ne4246)* mutant. **(A)** Embryonic lethality of *gfp::par-2* and *pkc-3(ne4246); gfp::par-2* embryos with the indicated depletions. The reported values correspond to the percentage of unhatched embryos over the total progeny (larvae and unhatched embryos) in all figures. *gfp::par-2; ctrl(RNAi)*, *n* = 4,975, *gfp::par-2; sds-22(RNAi)*, *n* = 3,923, *pkc-3(ne4246); gfp::par-2; ctrl(RNAi)*, *n* = 2,247, and *pkc-3(ne4246); gfp::par-2; sds-22(RNAi)*, *n* = 1,611. *gfp::par-2; szy-2(RNAi)*, *n* = 3,550; *pkc-3(ne4246); gfp::par-2; szy-2(RNAi)*, *n* = 2,588. *gfp::par-2; ape-1(RNAi)*, *n* = 720; *pkc-3(ne4246); gfp::par-2; ape-1(RNAi)*, *n* = 930. *sds-22(RNAi)* and *ape-1(RNAi)*, *N* = 3. *szy-2(RNAi)*, *N* = 4. The mean is shown and error bars indicate Standard Deviation (SD). The P values were determined using two-way ANOVA Tukey's multiple comparisons test. For plots of embryonic lethality, each dot inside the bar represents the average lethality of each independent experiment, unless otherwise indicated. **(B)** Representative frames of time-lapse videos of embryos at the pronuclear meeting stage: *gfp::par-2*; *ctrl(RNAi)*, *n* = 12

154 (PAR-2 is posterior in 100% of them), *gfp::par-2; sds-22(RNAi), n* = 12 (100% posterior PAR-2), *pkc-*
155 *3(ne4246); gfp::par-2; ctrl(RNAi), n* = 42 (0% posterior PAR-2, PAR-2 is all around the cortex in all
156 of them), and *pkc-3(ne4246); gfp::par-2; sds-22(RNAi*), *n* = 48 (87.5% have PAR-2 enriched in the
157 posterior cortex). *N* = 5. **(C)** GFP::PAR-2 intensity line profile along half of the embryo cortex starting
158 from the anterior, as shown in the scheme on the right. *pkc-3(ne4246); gfp::par-2; ctrl(RNAi), n* = 31,
159 *pkc-3(ne4246); gfp::par-2; sds-22(RNAi), n* = 32. *N* = 5. **(D)** Quantification of the GFP::PAR-2 domain
160 size at pronuclear meeting in live embryos with the indicated RNAi conditions. Sample size (*n*) is
161 indicated inside the bars in the graph. *N* = 4. Mean is shown and error bars indicate SD. The P values
162 were determined using one-way ANOVA. In C and E, each dot represents a single embryo. **(E)** Still
163 images of two-cell embryos of the indicated genotypes taken from DIC time-lapse movies. **(F)**
164 Quantification of the AB cell size as a percentage of the whole embryo size. Sample size (*n*) is indicated
165 inside the bars in the graph. *N* = 3. Mean is shown and error bars indicate SD. The P-values were
166 determined using two-way ANOVA "Tukey's multiple comparisons test". For all the panels, RNA
167 interference was performed by feeding. Scale bar is 10 µm, anterior is to the left and posterior to the
168 right. In all plots, ns $p > 0.05$, * $p < 0.05$, ** $p < 0.01$, ***$p < 0.001$, ****$p < 0.0001$, *n* = number of
169 embryos analyzed; *N* = number of independent experiments.
170

171 Polarity controls the posterior positioning of the mitotic spindle, which results in an asymmetric cell
172 division producing a larger anterior AB cell and a smaller posterior P1 cell. In *gfp::par-2* embryos AB
173 cell accounts for 56.5% of the total embryo length. In contrast, polarity defects in the *pkc-3(ne4246)*
174 mutant lead to reduced cell size asymmetry with a smaller AB cell, occupying 54.2% of the embryo
175 length. Consistent with the suppression of PAR-2 polarity defect, depletion of SDS-22 in *pkc-3(ne4246)*
176 embryos resulted in a bigger AB cell (57.1% embryo length), comparable to the size of AB in control
177 *gfp::par-2* embryos (Fig 1E,F).
178 Our data show that depletion of SDS-22 results in a smaller PAR-2 domain, partially suppresses the
179 polarity defects of a *pkc-3* temperature sensitive strain and the aberrant PAR-2 localization observed in
180 the PAR-2(L165V) mutant strain. As SDS-22 is a conserved PP1 regulator, our data suggest that SDS-
181 22 positively regulates GSP-2.
182

183 **The conserved E153 of SDS-22 is important for SDS-22 interaction with GSP-1 and GSP-2**
184 We have identified SDS-22 in immunoprecipitation with GSP-2 from embryos, thereby confirming a
185 previous finding that SDS-22 immunoprecipitates with both GSP-1 and GSP-2 from full worm lysates
186 (Peel *et al.*, 2017). We were able to confirm the interaction of SDS-22 with both GSP-1 and GSP-2 in
187 a two-hybrid assay (Fig 2).
188 SDS-22 is a leucine-rich repeat (LRR) protein and does not contain the degenerate RLxF PP1 docking
189 motif that has been found in most PP1 regulators. Instead, a conserved glutamic acid E153 in the LRR
190 domain is important for its interaction with the PP1 catalytic subunits (Fig 2) (Ceulemans *et al*, 2002;
191 Eiteneuer *et al*, 2014; Heroes *et al*, 2019). This site is conserved in *C. elegans* and we asked whether it
192 is important for the interaction of SDS-22 with GSP-1 and GSP-2. Substitution of the glutamine E153
193 with Alanine (referred to as SDS-22(E153A)) abrogated the interaction with both GSP-1 and GSP-2 in
194 the two-hybrid assays (Fig 2).

195 These data confirm that SDS-22 interacts with both GSP-1 and GSP-2 and identify the glutamic acid
196 residue E153 in the LRR domain of SDS-22 as crucial for the interaction, consistent with what has been
197 demonstrated for the human orthologs (Ceulemans *et al.*, 2002; Eiteneuer *et al.*, 2014; Heroes *et al.*,
198 2019).
199

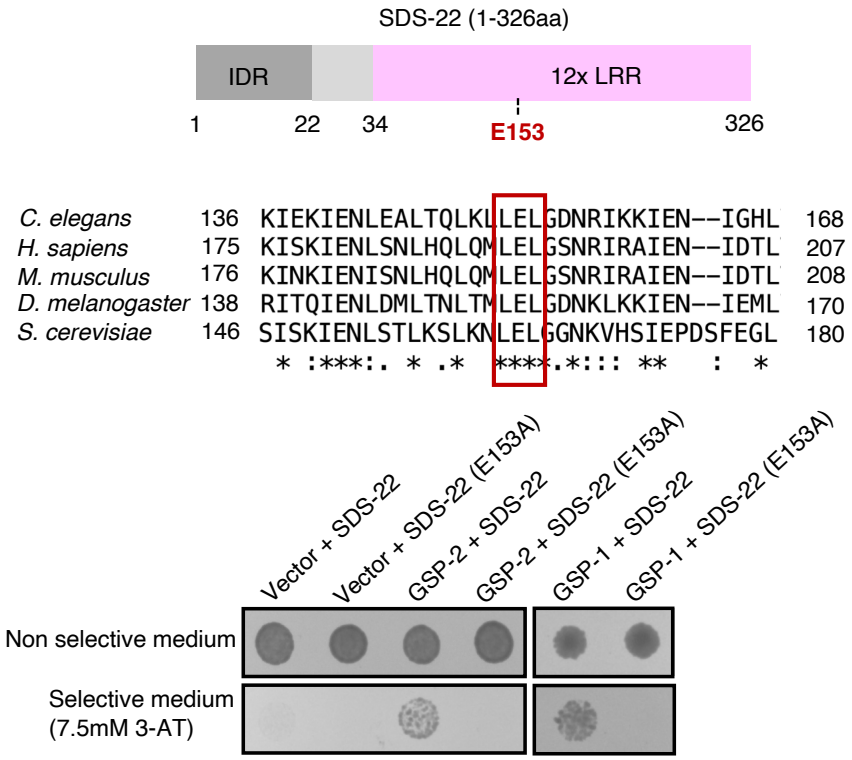

200

201 **Fig 2: SDS-22 interacts with GSP-1 and GSP-2 via the conserved E153 residue.**
202 Upper panel: schematic representation of the full-length (1-326aa) SDS-22. IDR: intrinsically
203 disordered region; LRR: leucine-rich repeats; E153: glutamic acid at amino acid residue 153. Middle
204 panel: sequence alignment of one PP1 interacting region in SDS22 from *C. elegans* (Uniprot P45969),
205 *H. sapiens* (Uniprot Q15435), *M. musculus* (Uniprot Q3UM45), *D. melanogaster* (Uniprot Q9VEK8),
206 and *S. cerevisiae* (Uniprot 936047). The reported PP1-binding residue E192 of *H. sapiens* is present in
207 *C. elegans* as E153, and this site is conserved in all species listed (marked by red square). Figure adapted
208 from alignment obtained with Uniprot alignment tool (https://www.uniprot.org/align). Lower panel:
209 yeast two-hybrid assays showing the interaction between SDS-22 (wild type and the E153A mutant)
210 and GSP-1 and GSP-2. Yeasts were transformed with the indicated plasmids (SDS-22 and
211 SDS-22(E153A) are fused to the DNA Binding Domain and GSP-1 and GSP-2 to the Activation
212 Domain) and were grown on non-selective and selective medium. Interaction between bait and prey
213 results in growth on selective medium (7.5mM 3-AT).
214

215 **Polarity defects are rescued in *pkc-3(ne4246); sds-22(E153A); gfp::par-2* embryos**

216 Our two-hybrid data show that SDS-22 interacts with GSP-1 and GSP-2 through the E153 residue. We
217 introduced this substitution in vivo and asked whether *sds-22(E153A)* mutant embryos display a smaller
218 PAR-2 domain, as observed in SDS-22 depleted embryos (Fig 1B,D). PAR-2 was restricted to the
219 posterior in *gfp::par-2; sds-22(E153A)* as in control embryos, but the length of the domain was

220 decreased (Fig 3A,B, Movie EV2), similar to what was observed in SDS-22 and GSP-2 depleted
221 embryos. However, while SDS-22 depletion resulted in 73.6% embryonic lethality (Fig 1A), *gfp::par-*
222 *2; sds-22(E153A)* only exhibited 5.3% embryonic lethality compared to the *gfp::par-2* strain (Fig 3C).
223 Because of this, we decided to test whether *sds-22(E153A)* was able to rescue the lethality and the
224 polarity defects of *pkc-3(ne4246)* embryos. We introduced the E153A mutation in *pkc-3(ne4246);*
225 *gfp::par-2* strain, let them grow at the semi-permissive temperature (24°C) and quantified embryonic
226 lethality. We found that the lethality of the embryos was not rescued at this temperature (Fig 3D).
227

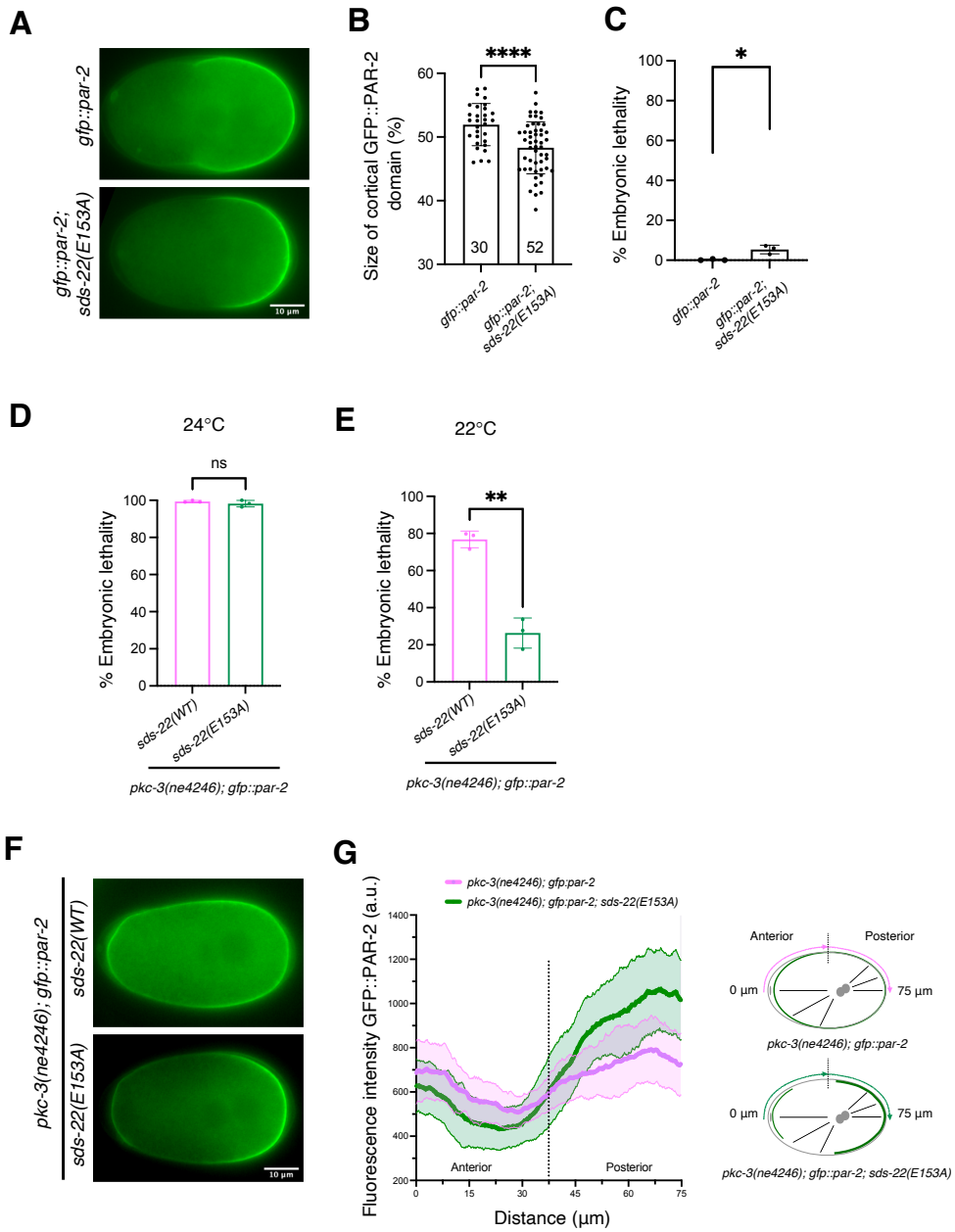

228

229 **Fig 3: Mutation of SDS-22 E153 residue partially rescues polarity defects of *pkc-3(ne4246)* mutant.**
230 **(A)** Still images at the pronuclear meeting stage from time-lapse videos of *gfp::par-2* and *gfp::par-2;*
231 *sds-22(E153A)*. **(B)** Quantification of the GFP::PAR-2 domain size at pronuclear meeting in live
232 zygotes. Sample size (*n*) is indicated inside the bars in the graph, each dot represents a single embryo.
233 *N* = 3. Mean is shown and error bars indicate SD. The P value was determined using two-tailed unpaired

Student's *t* test. **(C)** Percentage of embryonic lethality of *gfp::par-2* and *gfp::par-2; sds-22(E153A). gfp::par-2, n* = 757, *gfp::par-2; sds-22(E153A), n* = 2644. *N* = 3. Mean is shown and error bars indicate SD. The P value was determined using two-tailed unpaired Student's *t* test. **(D, E)** Percentage of embryonic lethality of *pkc-3(ne4246); gfp::par-2* and *pkc-3(ne4246); gfp::par-2; sds-22(E153A)* at the semi-permissive temperature of 24°C **(D)** and of 22°C **(E)**. For **(D)**, *pkc-3(ne4246); gfp::par-2*, *n* = 569, and *pkc-3(ne4246); gfp::par-2; sds-22(E153A), n* = 545. For **(E)**, *pkc-3(ne4246); gfp::par-2*, *n* = 2171, and *pkc-3(ne4246); gfp::par-2; sds-22(E153A) n* = 1867. *N* = 3. Mean is shown and error bars indicate SD. The P value was determined using two-tailed unpaired Student's *t* test. In C, D and E, dots represent the mean lethality of each independent experiment. **(F)** Still images from time-lapse videos of *pkc-3(ne4246); gfp::par-2* and *pkc-3(ne4246); gfp::par-2; sds-22(E153A)* embryos at the pronuclear meeting stage. Worms were grown at the semi-permissive temperature of 22°C as in panel E. **(G)** GFP::PAR-2 intensity line profile along half of the embryo cortex starting from the anterior, as shown in the scheme on the right. *pkc-3(ne4246); gfp::par-2* and *pkc-3(ne4246); gfp::par-2; sds-22(E153A)* *n* = 19 for both genotypes. *N* = 3. Worms were grown at the semi-permissive temperature of 22°C as in panel E and F. Scale bar is 10 µm, anterior is to the left and posterior to the right. In all plots, ns $p > 0.05$, * $p < 0.05$, ** $p < 0.01$, ***$p < 0.001$, ****$p < 0.0001$, *n* = number of embryos analyzed; *N* = number of independent experiments.

Decreasing the temperature to 22°C reduced the embryonic lethality in the *pkc-3(ne4246); gfp::par-2* strain (Fig 3E) to about 76.8%. In these more permissive conditions, *pkc-3(ne4246); sds-22(E153A); gfp::par-2* exhibited only 26.4% embryonic lethality, indicating that the *sds-22(E153A)* mutation, which abolishes SDS-22 interaction with GSP-1/-2, can partially rescue the lethality of *pkc-3(ne4246)* at this temperature.

When we looked at polarity we found that PAR-2, despite still weakly detectable at the anterior, was more enriched at the posterior cortex in the *pkc-3(ne4246); sds-22(E153A); gfp::par-2* mutant embryos compared to *pkc-3(ne4246); gfp::par-2* (Fig 3F,G, Movie EV 3). The rescue of embryonic lethality and polarity phenotypes was not due to a reduced expression level of SDS-22(E153A) because SDS-22(E153A)::GFP showed similar protein intensity as SDS-22::GFP (Fig EV4).

Our data show that a mutation that disrupts the interaction of SDS-22 with GSP-1 and GSP-2 in a two-hybrid assay, can lead to a partial rescue of the lethality and the polarity defect of *pkc-3(ne4246); gfp::par-2* embryos, suggesting that the interaction of SDS-22 with the PP1 phosphatases contributes to polarity establishment.

Loss or mutation of SDS-22 results in hyper-phosphorylation of a PP1 substrate

In *C. elegans* embryos GSP-1 and GSP-2 redundantly regulate PAR-2 localization (Calvi *et al.*, 2022). GSP-2 is the predominant PP1 phosphatase that allows for PAR-2's localization to the posterior cortex. Depletion of GSP-2 reduces the size of the PAR-2 domain in the *gfp::par-2* strain while depletion of GSP-1 does not lead to observable defects in PAR-2 domain size. Only when GSP-1 and GSP-2 are co-depleted, PAR-2 remains mostly cytoplasmic (Fig 4A, (Calvi *et al.*, 2022)). If SDS-22 was essential to regulate the activity of both GSP-1 and GSP-2, its depletion should result in a loss of PAR-2 cortical localization, similar to what is observed in the co-depletion of GSP-1 and GSP-2. As shown above, depletion of SDS-22 in the *gfp::par-2* strain did not lead to cytoplasmic localization of PAR-2 (Fig 1B

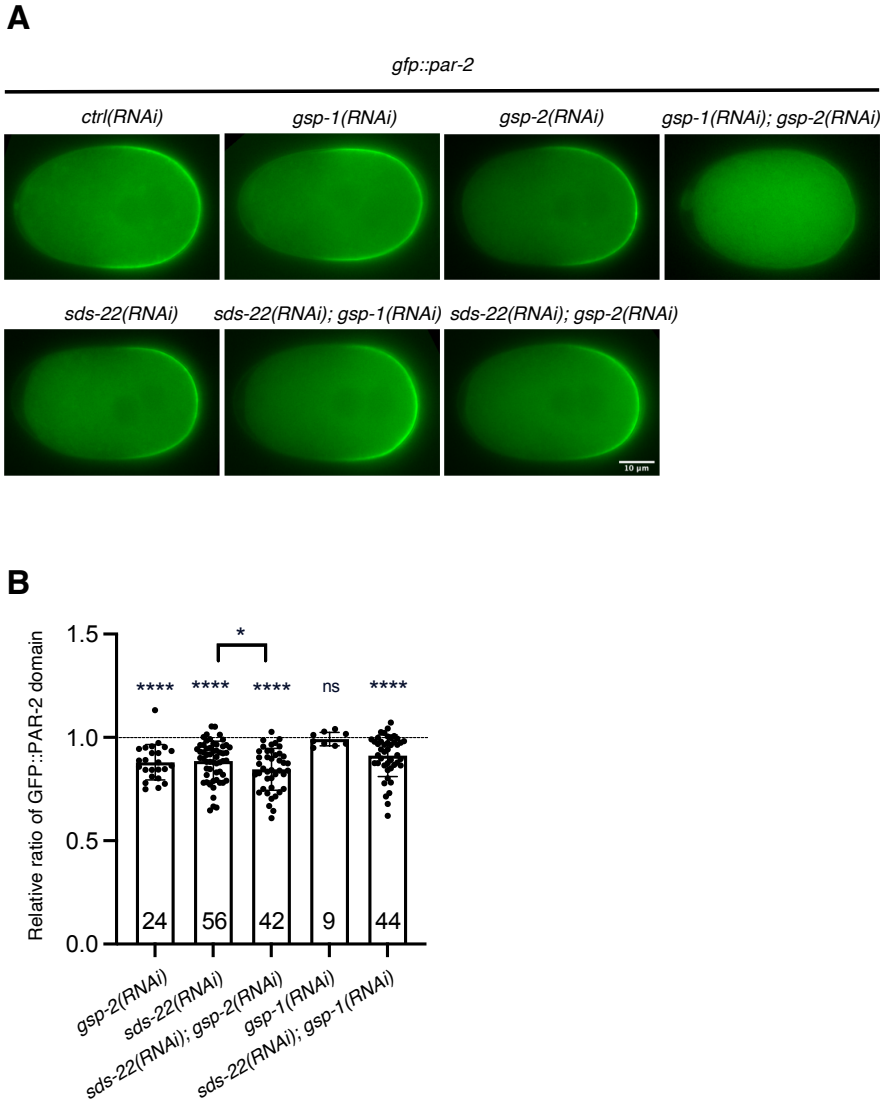

Fig 4: SDS-22 does not genetically regulate GSP-1, GSP-2 or both.
(A) Still images from time-lapse videos of *gfp::par-2* zygotes at pronuclear meeting with the indicated depletions. RNA interference was performed by injection. Scale bars is 10 µm, anterior is to the left and posterior to the right. **(B)** Quantification of the relative ratio of GFP::PAR-2 size domain with indicated RNAi conditions. Each condition was compared to *ctrl(RNAi)* treatment within the same experiment. The P value was determined using two-tailed unpaired Student's *t* test. Sample size (*n*) is indicated inside the bars in the graph. $N = 4\text{-}5$. Mean is shown and error bars indicate SD. ns $p > 0.05$, * $p < 0.05$, ** $p < 0.01$, ***$p < 0.001$, ****$p < 0.0001$.

and 4A) but resulted in a smaller PAR-2 domain (Fig 1D and 4B), as observed in the GSP-2 depletion. These data suggest that SDS-22 regulates GSP-2 rather than GSP-1. If this was true, depletion of both SDS-22 and GSP-1 should result in PAR-2 remaining in the cytoplasm, similar to GSP-1 and GSP-2 co-depletion. We therefore co-depleted SDS-22 and GSP-1 and, as control, SDS-22 and GSP-2. The double depletion was efficient as shown in Fig EV5. In embryos co-depleted of SDS-22 and GSP-1, PAR-2 still formed a posterior cortical domain. Co-depletion of SDS-22 and GSP-2 resulted in an even more pronounced reduction of PAR-2 domain compared to the single depletion of SDS-22 (Fig 4A,B), suggesting that SDS-22 plays a different role than simply activating GSP-2 (see below).

Our findings show that depletion or mutation of SDS-22 partially rescues polarity defects of the *pkc-3(ne4246)* mutant. However, neither SDS-22 depletion alone nor co-depletion with GSP-1 or GSP-2 prevents PAR-2 cortical localization similar to GSP-1/-2 co-depletion. To understand the role of SDS-22 in the regulation of GSP-1 and GSP-2, we investigated whether SDS-22 depletion or mutation decreases PP1 activity. To quantify the activity of the PP1 phosphatase, we examined the phosphorylation levels of a well characterized substrate, histone H3, as previously described (Hsu *et al.*, 2000; Qian *et al*, 2011). Histone H3 is phosphorylated at the Ser 10 residue by the Aurora B kinase in the early phases of mitosis and it is dephosphorylated by PP1 at anaphase (Xin *et al*, 2020). We found that phospho-histone H3 (Ser10) levels on the chromosomes during anaphase were higher in SDS-22 depleted one-cell embryos (Fig 5A) compared to control depletion, indicating that depletion of SDS-22 leads to deficient dephosphorylation of PP1 substrates.

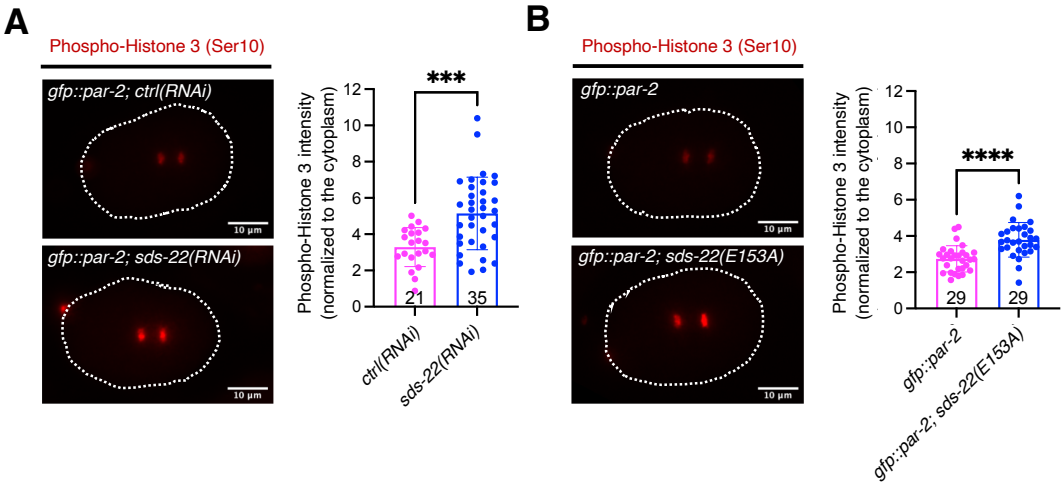

Fig 5. Loss or mutation of SDS-22 decreases GSP-1 and GSP-2 activity.
(A) Left, images of a *gfp::par-2; ctrl(RNAi)* anaphase embryo and a *gfp::par-2; sds-22(RNAi)* anaphase embryo stained for phospho-histone H3 (Ser10) (in red). Right, quantifications. **(B)** Left, images of a *gfp::par-2* and a *gfp::par-2*; *sds-22(E153A)* embryo at anaphase stained for phospho-histone H3(Ser10) (in red). Right, quantifications. For both **A** and **B**, sample size (*n*) is indicated inside the bars in the graph, each dot represents an embryo. $N = 4$. Phospho-histone H3 (Ser10) intensity was normalized to cytoplasmic levels. The P-values were determined using two-tailed unpaired Student's t-test. ***$p < 0.001$, ****$p < 0.0001$. The dashed lines indicate the outline of embryos. RNA interference was performed by feeding. Scale bar is 10 µm.

Similar to the observation in SDS-22 depleted embryos (Fig 5A), phospho-histone H3 (Ser10) levels were higher in the *sds-22(E153A)* mutant embryos (Fig 5B), suggesting that the interaction between SDS-22 and GSP-1 and GSP-2 is important to maintain efficient dephosphorylation of a PP1 substrate. To conclude, while our genetic data on PAR-2 cortical localization suggest that SDS-22 is not required to fully activate GSP-1 and/or GSP-2, depletion or mutation of SDS-22 results in a reduced activity of the phosphatases, as shown by phospho-histone H3 (Ser10) levels. This suggests that SDS-22 plays a general role in regulating GSP-1 and GSP-2, which is not specific to cell polarity.

323 **SDS-22 maintains GSP-1 and GSP-2 protein levels by protecting them from proteasomal**
324 **degradation**
325 Regulatory subunits of phosphatases can regulate their activity, localization or protein levels (Aggen *et*
326 *al.*, 2000; Verbinnen *et al.*, 2017; Virshup & Shenolikar, 2009). Recent work in human cells and in
327 vitro has shown that SDS22 coordinates the assembly of the PP1 holoenzyme (Cao *et al.*, 2024; Kueck
328 *et al.*, 2024). To understand how SDS-22 contributes to the function of GSP-1 and GSP-2, we
329 investigated whether SDS-22 regulated the localization or levels of GSP-1 and GSP-2. We depleted
330 SDS-22 in the *mNG::gsp-2* and *gfp::gsp-1* strains and observed that the localization of GSP-2 and GSP-
331 1 was not altered by SDS-22 depletion (Fig 6A). However, the intensity of mNG::GSP-2 and
332 GFP::GSP-1 dropped to 53.7% and 59.5% compared to the control strains (Fig 6B,C). This result was
333 confirmed by western blot analysis (Fig 6D,E). SDS-22 is therefore essential to maintain the proper
334 levels of GSP-1 and GSP-2 in *C. elegans* embryos.
335 We next asked whether SDS-22 maintains GSP-1 and GSP-2 levels in vivo via their physical interaction
336 with the proteins. We generated strains in which the E153 site of SDS-22 is mutated in the genetic
337 background of *mNG::gsp-2* and *gfp::gsp-1* separately. In contrast to the low lethality observed in
338 *sds-22(E153A)* mutant in the *gfp::par-2* genetic background (Fig 3C), *sds-22(E153A)* mutation caused
339 99.1% embryonic lethality in *mNG::gsp-2* and 32.3% in *gfp::gsp-1* (Fig EV6A,B). These data suggest
340 that tagged GSP-2 and GSP-1 strains are hypomorph even though there are no observable growth
341 defects nor embryonic lethality in these strains. Because of the high embryonic lethality of *mNG::gsp-*
342 *2; sds-22(E153A)* homozygous mutant, we maintained the strain as a *sds-22(E153A)* heterozygote (see
343 methods). Consistent with the phenotypes of *sds-22(RNAi)*, SDS-22(E153A) mutation led to a 46.3%
344 of reduction of the mNG::GSP-2 intensity (Fig 6F,G) and to a 21% reduction of the GFP::GSP-1
345 intensity (Fig 6F,H).
346 We then investigated whether the levels of GSP-1 and/or GSP-2 affected the levels of SDS-22. We
347 performed single depletion and co-depletion of GSP-1 and GSP-2 in *sds-22::gfp* strain. We found that
348 the levels of SDS-22 were weakly reduced by single depletion of GSP-1 or GSP-2 (around 8% of
349 reduction in both conditions), but were un-affected by co-depletion of both GSP-1 and GSP-2 (Fig
350 EV7A,B).
351
352
353
354

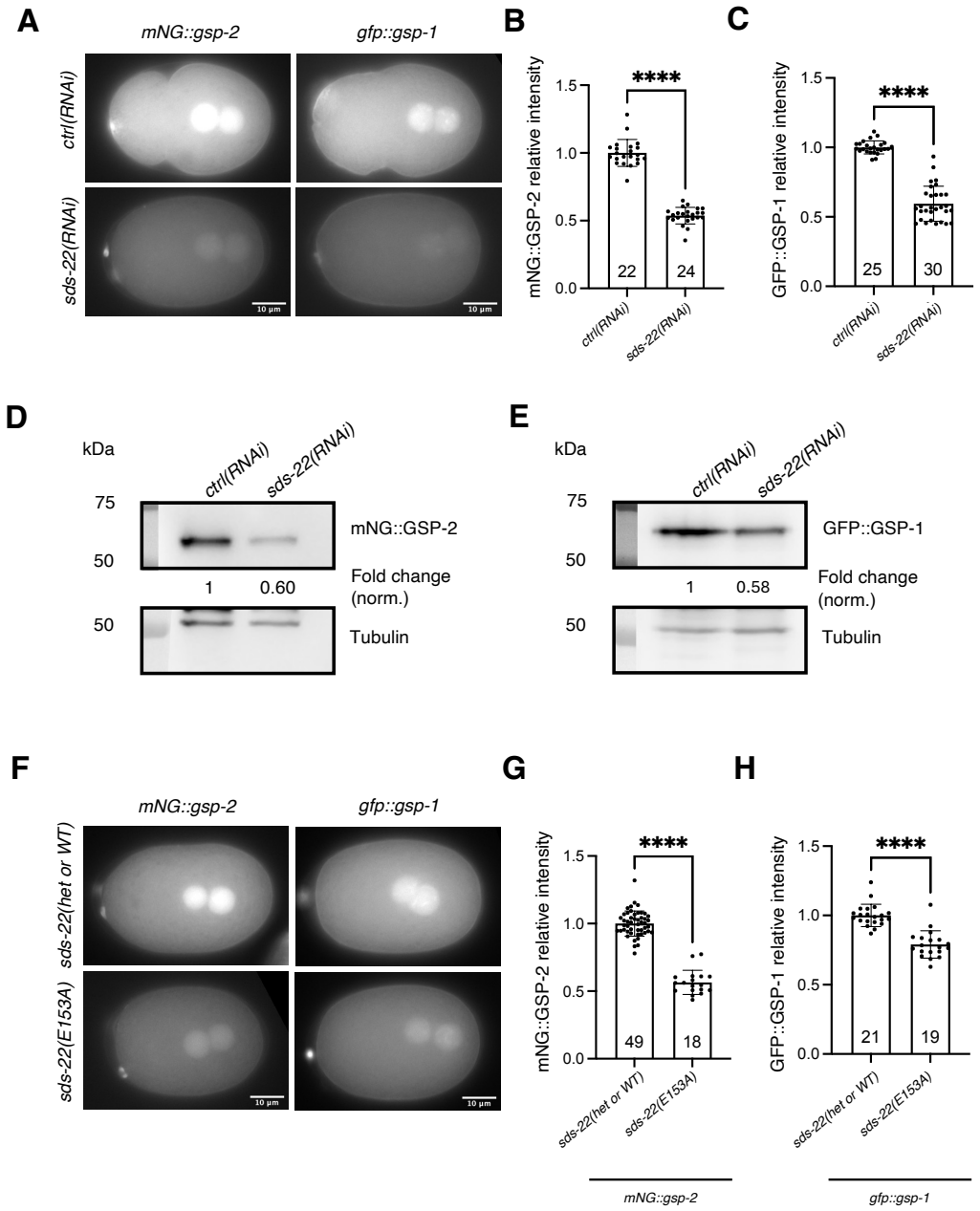

Fig 6: SDS-22 depletion or mutation causes a reduction of GSP-1 and GSP-2 protein levels. **(A)** Representative images of *mNG::gsp-2* and *gfp::gsp-1* embryos in *ctrl(RNAi)* and *sds-22(RNAi)*. **(B, C)** Quantification of relative mNG::GSP-2 **(B)** and GFP::GSP-1 **(C)** levels in *sds-22(RNAi)* normalized to *ctrl(RNAi)*. Mean is shown and error bars indicate SD. $N = 4$. ****p < 0.0001. **(D, E)** Western Blot of embryonic extracts from *mNG::gsp-2* **(D)** and *gfp::gsp-1* **(E)** in *ctrl(RNAi)* and *sds-22(RNAi)* embryos. Tubulin is used as a loading control. Fold change of mNG::GSP-2 and GFP::GSP-1 normalized to Tubulin levels were shown below the Western blot image. $N = 1$. **(F)** Representative images of *mNG::gsp-2; sds-22(E153A/+ or +/+,* a mixture of wild type and heterozygous of the E153A mutant, see methods), *mNG::gsp-2; sds-22(E153A), gfp::gsp-1* and *gfp::gsp-1; sds-22(E153A).* **(G, H)** Quantification of relative mNG::GSP-2 **(G)** and GFP::GSP-1 **(H)** levels with SDS-22(E153A) mutation normalized to wild type. *mNG::gsp-2,* $N = 3$. *gfp::gsp-1,* $N = 4$. ****p < 0.0001. In A-E, RNA interference was performed by feeding. In **B**, **C**, **G**, **H**, mean is shown, error bars indicate SD, the P-values were determined using two-tailed unpaired Student's t-test. Dots in graphs represent individual embryo measurements and sample size (*n*) is indicated inside the bars in the graph.

370 In budding yeast, when Sds22 is mutated, PP1-Glc7 is prone to misfold and form aggregates with heat-
371 shock proteins, which are cleared by the proteasome (Cheng & Chen, 2015). Additionally, in human
372 cells, SDS22 stabilizes nascent PP1 (Cao *et al.*, 2024). We hypothesized that GSP-1 and GSP-2 are
373 degraded by the proteasome when SDS-22 is depleted or mutated. To test this hypothesis, we reduced
374 proteasomal activity in SDS-22-depleted or mutated embryos by depleting the proteasomal subunits
375 RPN-6.1 or RPN-7, which localize to the 19S regulatory complex and are essential for the proteolytic
376 activity (Fernando *et al*, 2022; Papaevgeniou & Chondrogianni, 2014). Since depletion of these subunits
377 results in worms with very little to no progeny (Fernando *et al.*, 2022), we analyzed the protein intensity
378 of GSP-1 and GSP-2 in the -1 and -2 oocytes in the germline and investigated whether reducing
379 proteasomal activity would restore GSP-1 and GSP-2 levels.
380 When RPN-6.1 or RPN-7 were depleted, there was an increase of GSP-1 and GSP-2 intensity both in
381 the cytoplasm and in the nucleus of the oocytes (Fig 7A-F, Fig EV8), indicating that GSP-1 and GSP-
382 2 are subject to proteasomal degradation in the germline of *C. elegans*. Consistent with the observation
383 in embryos (Fig 6A), both cytoplasmic and nuclear GSP-2 levels in the germline were reduced by about
384 50% after depletion of SDS-22 (Fig 7B,C). Importantly, when SDS-22 was depleted together with
385 RPN-6.1 or RPN-7, the levels of GSP-2 were restored (Fig 7A-C, Fig EV8A). The efficiency of SDS-
386 22 depletion in the RPN-6.1 or RPN-7 co-depletion was verified (Fig EV9). In *sds-22(RNAi)* oocytes,
387 the levels of GFP::GSP-1 exhibited a smaller decrease (17.4%) in the nucleus and an even smaller
388 reduction in the cytoplasm, which was not statistically significant (8.8%, n.s.) (Fig 7D-F). The reduced
389 nuclear and cytoplasmic intensities of GSP-1 following SDS-22 depletion were also rescued by co-
390 depletion of RPN-6.1 or RPN-7 (Fig 7D-F, Fig EV8B), similar to the recovery of GSP-2 levels (Fig
391 7B,C). To further test the role of SDS-22 on GSP-1 stability, we measured GFP::GSP-1 levels in the -
392 1 and -2 oocytes in the *gfp::gsp-1; sds-22(E153A)* strain. In the germline of *gfp::gsp-1; sds-22(E153A)*
393 worms, GSP-1 levels were reduced (28.8% in the cytoplasm; 31.0% in the nucleus) (Fig 7G-I). In the
394 same mutant, depletion of RPN-6.1 or RPN-7 increased the levels of GSP-1 (Fig 7G-I, Fig EV8C),
395 supporting our hypothesis that SDS-22, through its interaction with GSP-1, protects GSP-1 from
396 proteasome mediated degradation. Since we use the embryonic lethality phenotype of the *mNG::gsp-2;*
397 *sds-22(E153A)* strain to recognize the homozygote *sds-22(E153A),* this precluded the possibility to
398 analyze the germlines of homozygote *mNG::gsp-2; sds-22(E153A)* worms depleted of RNP-6.1 or
399 RPN-7, as these worms do not have progeny (Fernando *et al.*, 2022) and we therefore cannot distinguish
400 the *sds-22(E153A)* homozygote from the *sds-22(E153A)* heterozygote (see material and methods for
401 details).
402 In summary, these data show that SDS-22 is important to maintain the levels of GSP-1 and GSP-2 by
403 protecting them from proteasome mediated degradation.

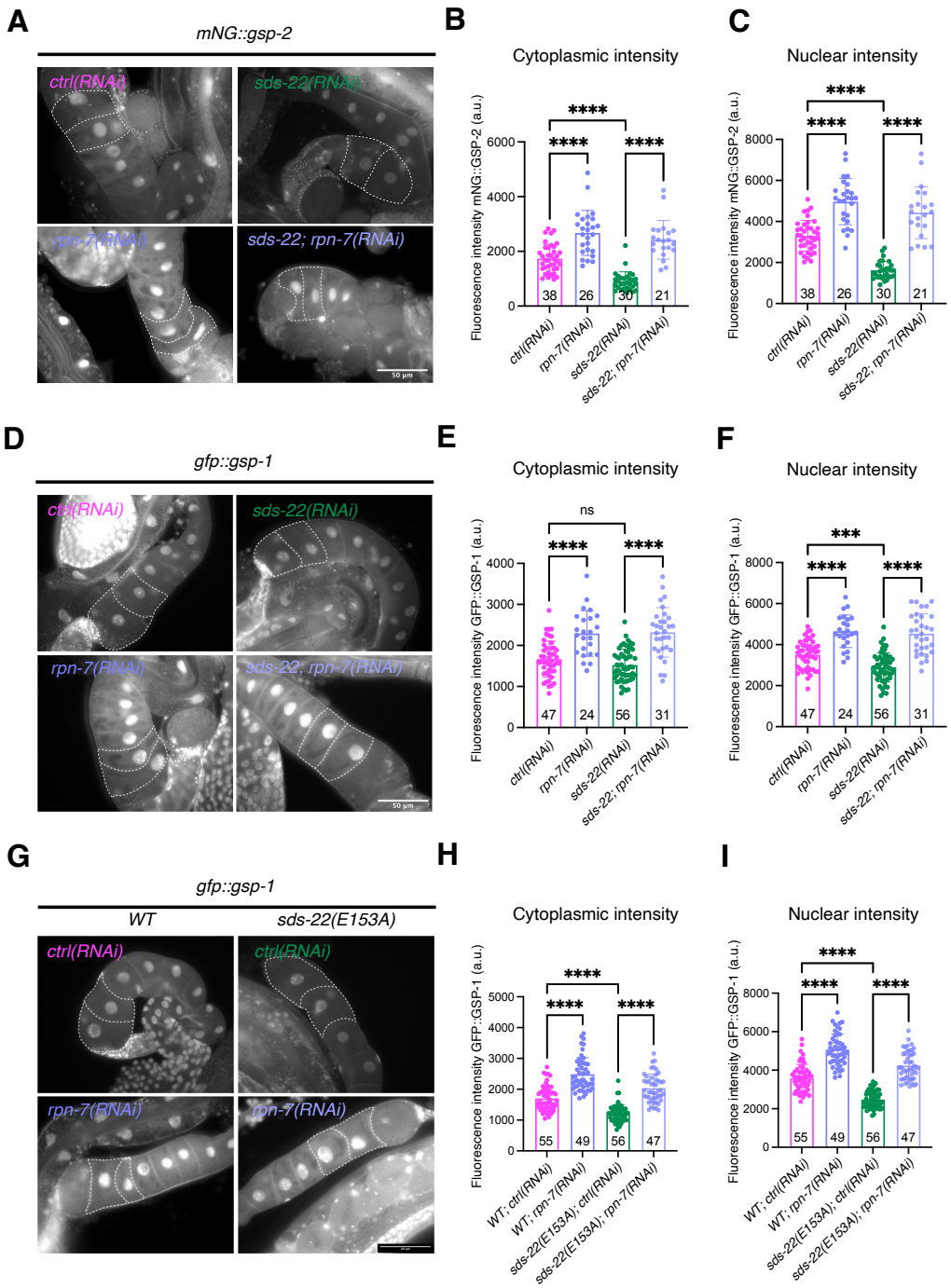

Fig 7: SDS-22 protects GSP-1 and GSP-2 from proteasomal degradation.
(A) Representative images of *mNG::gsp-2* germlines in *ctrl(RNAi), sds-22(RNAi), rpn-7(RNAi)* and *sds-22(RNAi); rpn-7(RNAi)*. **(B, C)** Quantification of mNG::GSP-2 intensity levels in the cytoplasm **(B)** and nucleus **(C)** of -1 and -2 oocytes. $N = 3$. **(D)** Representative images of *gfp::gsp-1* germlines in *ctrl(RNAi), sds-22(RNAi), rpn-7(RNAi)* and *sds-22(RNAi); rpn-7(RNAi)*. **(E, F)** Quantification of GFP::GSP-1 intensity levels in the cytoplasm **(E)** and nucleus **(F)** of -1 and -2 oocytes. $N = 3$. **(G)** Representative midsection images of *gfp::gsp-1, gfp::gsp-1;sds-22(E153A)* germlines in *ctrl(RNAi)* and *rpn-7(RNAi)*. **(H, I)** Quantification of GFP::GSP-1 intensity levels in the cytoplasm **(H)** and nucleus **(I)** of -1 and -2 oocytes. $N = 3$. For **B**, **C**, **E**, **F**, **H** and **I**, mean is shown and error bars indicate SD. Each dot represents the measurement of one germline. The P-values were determined using one-way ANOVA "Tukey's multiple comparisons test". Sample size (n) is indicated inside the bars in the graph. For all panels, RNA interference was performed by feeding. The scale bars are 50 µm. In all plots, ns $p > 0.05$, * $p < 0.05$, ** $p < 0.01$, ***$p < 0.001$, ****$p < 0.0001$, n = number of embryos analyzed; N = number of independent experiments.

419 **Discussion**
420
421 Cell polarity establishment in the *C. elegans* embryos is crucial for subsequent asymmetric cell
422 divisions and later development. Previous studies have shown that the balanced activity of the kinase
423 PKC-3 and the PP1 phosphatases GSP-1 and GSP-2 is essential for the posterior cortical localization
424 of PAR-2 (Calvi *et al.*, 2022; Hao *et al.*, 2006; Motegi *et al.*, 2011). GSP-1/-2 are PP1 catalytic subunits
425 that rely on regulatory subunits to direct their cellular localization or facilitate their activity within a
426 functional holoenzyme. Here we find that a conserved PP1 regulator, SDS-22, when depleted, results
427 in a smaller PAR-2 domain and can partially rescue the polarity defects of a *pkc-3(ne4246)* mutant. We
428 demonstrate that SDS-22 contributes to the activity of GSP-1/-2 by protecting them from proteasomal
429 degradation and maintaining their protein levels. Taken together, our data suggest that the role of SDS-
430 22 in polarity is indirect via the regulation of GSP-1/-2 levels. In support of this, SDS-22 depletion
431 results in broader GSP-1/-2 dependent phenotypes such as increased Phospho-H3 (Ser10) (Fig 5) and
432 centriole duplication defects in later-stage embryos (Peel *et al.*, 2017).
433 SDS-22 is a conserved protein previously shown to be important for cell polarity. In *Drosophila,* Sds22
434 is essential for maintaining the morphology and apical-basal polarity of follicle epithelial cells (Grusche
435 *et al*, 2009) and it facilitates the cortical localization of the lethal giant larvae (Lgl) protein in these cells
436 (Moreira *et al.*, 2019). In mammalian and yeast cells, SDS22 is required for mitotic progression (Duan
437 *et al.*, 2016; Posch *et al.*, 2010; Wurzenberger *et al.*, 2012). Even though SDS22 appears as a conserved
438 regulator of PP1 phosphatases, the exact mechanism by which SDS22 regulates PP1 activity was still
439 debated. Some studies have shown that SDS22 positively contributes to PP1 activity in mitosis
440 (MacKelvie *et al*, 1995; Stone *et al*, 1993) and plays a role in localizing PP1 and in protein folding of
441 the PP1 complex (Cheng & Chen, 2015; Peggie *et al.*, 2002). However, other studies suggested that
442 SDS22 inhibits PP1 activity in vitro (Lesage *et al.*, 2007). Two recent studies from the Bollen and
443 Meyer groups show that SDS22 plays a key role in the biogenesis of PP1 holoenzymes (Cao *et al.*, 2024;
444 Kueck *et al.*, 2024). On the one hand, SDS22 stabilizes newly translated PP1; on the other hand, SDS22
445 and Inhibitor 3 (I3) bind to PP1, forming a ternary complex that inhibits PP1 activity. This inhibitory
446 complex is dissociated by the AAA ATPase p97/Valosin, allowing PP1 to bind canonical regulatory
447 subunits to form a functional holoenzyme. Given that SDS-22 both stabilizes PP1 levels and inhibits its
448 activity, this dual role clarifies the apparent contradiction: while SDS-22 is essential for PP1 activity in
449 vivo (because it is essential for the biogenesis/stability), it inhibits PP1 activity in vitro (as it needs to
450 be removed to have an active PP1), while in vivo it is removed by p97/Valosin resulting in active PP1
451 (Cao *et al.*, 2024; Kueck *et al.*, 2024).
452 Our data in *C. elegans* support and complement these studies. We show that SDS-22 is not essential for
453 full activation of both GSP-1 and GSP-2, since depletion of SDS-22 does not abolish polarity, as
454 observed in the co-depletion of GSP-1 and GSP-2 (Calvi *et al.*, 2022). Embryos co-depleted of SDS-22
455 and GSP-1 or of SDS-22 and GSP-2, are also able to polarize, indicating that SDS-22 plays a different

role than simply activating GSP-1, GSP-2 or both. We find that in *C. elegans* SDS-22 is required to maintain the appropriate levels of both GSP-1 and GSP-2. We propose that the reduced levels of GSP-2 explain why loss of SDS-22 partially rescues PAR-2 defect in *pkc-3(ne4246)* mutant allele on one side (Fig 1B). On the other side, since embryos still have GSP-1 and GSP-2 proteins they are able to polarize after the depletion of SDS-22, or co-depletion of SDS-22 with GSP-1 or SDS-22 with GSP-2 in *gfp::par-2* embryos (Fig 4). In these conditions, depletion of SDS-22, whether alone or in conjunction with GSP-1 or GSP-2, only results in a partial loss of the PP1 subunits GSP-1 and/or GSP-2 and in a reduction in catalytic activity. Consistent with GSP-2 reduced levels, SDS-22 depleted or E153A mutant embryos also have a smaller PAR-2 domain. However, since these embryos also show reduced cortical ruffling (Movie EV1,2) and are smaller (Fig EV2C) we cannot exclude that these two phenotypes also contribute to the smaller size of the PAR-2 domain.

How SDS-22 maintains PP1 level has not been fully clarified. In budding yeast, it has been reported that when Sds22 is mutated, PP1/Glc7 forms aggregates in the nucleus, despite the overall protein level remaining unaltered (Peggie *et al.*, 2002). These aggregates co-localize with heat-shock proteins that require clearance by the proteasome (Cheng & Chen, 2015). Co-expression of PP1 with chaperones GroEL/ES(HSP-60) in bacteria (Peti *et al*, 2013) or with SDS22 in mammalian cells (Choy *et al*, 2019) increases PP1 yield and solubility. These findings suggest that in the absence of SDS22, PP1 is prone to mislocalization or misfolding, leading to aggregation. Interestingly, Peel et al. found SDS-22 co-immunoprecipitated with TCP-1 and HSP-60 (Peel *et al.*, 2017), both members of the chaperonin family critical for protein folding (Hayer-Hartl *et al*, 2016; Kubota *et al*, 1995). Collectively, these findings suggest that by facilitating protein folding SDS22 protects PP1 from degradation. In the *C. elegans* germline and embryos GSP-1/-2 do not form visible aggregates when SDS-22 is depleted but they undergo degradation in a proteasome-dependent manner (Fig 7). Our data, together with previous findings (Cao *et al.*, 2024; Cheng & Chen, 2015), demonstrate a role of SDS-22 in protecting PP1s from proteasomal degradation. Interestingly, E153A mutation of SDS-22 affected GSP-2 levels much more strongly than GSP-1 levels in embryos (Fig 6F-H). Furthermore, in germlines, GSP-1 levels were less affected by loss of SDS-22 (Fig 7). This indicates that GSP-2 is more susceptible to the interaction with SDS-22.

Our data and the recent studies of the Bollen and Meyer laboratories (Cao *et al.*, 2024; Kueck *et al.*, 2024) suggest that there is a canonical regulator of GSP-1 and GSP-2 in embryonic polarity that we have not yet identified. In the immunoprecipitations of GSP-2 from embryos we have identified APE-1 and SZY-2(I-2). APE-1 has been shown to direct GSP-2, but not GSP-1, localization to epidermal junctions and modulate GSP-2 activity (Beacham *et al.*, 2022). SZY-2(I-2) regulates both GSP-1/-2 in centriole duplication from the four-cell stage of *C. elegans* embryos (Peel *et al.*, 2017). However, our data suggest that neither APE-1 nor SZY-2 functions as canonical PP1 regulators in PAR-2's regulation, as depletion of either did not rescue the polarity defects of *pkc-3(ne4246)* mutant (Fig 1A, EV2A). We cannot exclude the possibility that SDS-22 may also function as a canonical regulator of the PP1

493 holoenzymes in controlling PAR-2 localization in *C. elegans* embryos. Further investigation is required
494 to determine whether a yet-to-be-identified regulator of the PP1 holoenzyme is responsible for loading
495 PAR-2 to the posterior cortex.
496 Another open question is if and how the activity of PP1 catalytic subunits is asymmetrically modulated
497 in the one-cell embryo. Our previous work (Calvi *et al.*, 2022) suggests that the activity of GSP-1/-2
498 might be asymmetrically restricted by the anterior-enriched polo-like kinase PLK-1, which
499 consequently gives rise to asymmetric posterior localization of PAR-2. One possibility is that PLK-1
500 directly phosphorylates and regulates the activity of GSP-1 and/or GSP-2. Interestingly, a recent study
501 shows that in *Drosophila* cells POLO kinase phosphorylates and inhibits PP1 (Moura *et al*, 2024).
502 However, we were not able as yet to identify potential phosphorylated sites that regulates PP1 activity
503 (our unpublished data). Another possibility is that PLK-1 regulates the regulatory subunit(s) of GSP-
504 1/-2. Notably, in mammalian cells, SDS22 is phosphorylated and inhibited by Plk1 during mitosis
505 (Duan *et al.*, 2016). Further studies will be required to understand whether additional pathways regulate
506 the activity of this phosphatase during polarity establishment.
507
508 **Material and Methods**
509
510 **Worm strains**
511 Worms were maintained on NGM plates seeded with OP50 bacteria using standard methods (Brenner,
512 1974). The strains used in this work are listed in Table S1. The strains containing the temperature
513 sensitive *pkc-3(ne4246)* mutation, *pkc-3(ne4246); gfp::par-2* (Ng *et al*, 2022) and *pkc-3(ne4246);*
514 *gfp::par-2; sds-22(E153A),* were kept at 15°C. All the other strains were maintained at 20°C.
515 Mutant strains were generated using CRISPR/Cas9 technology as described (Arribere *et al*, 2014). The
516 single guide RNAs, repair templates used to generate the mutants, PCR primers used to amplify the
517 sequence with mutation, as well as enzymes used for the screening, are listed in Table S2-4. For the
518 strain ZU341 *(gfp::par-2; sds-22(E153A))*, two independent isolates were analyzed. The ZU362
519 *mNG::gsp-2; sds-22(E153A)* was maintained as a *sds-22(E153A)* heterozygote. *mNG::gsp-2; sds-*
520 *22(E153A)* adult worms are viable but produce 100% dead progeny, indicating that this mutation
521 behaves as a maternal effect lethal in the *mNG::gsp-2* background.
522
523 **RNA interference**
524 Clones from the Ahringer feeding library (Ahringer, 2006; Kamath *et al*, 2003) were used as listed in
525 Table S5. The clone C06A6.2 served as the control for the injection experiments, as previously done
526 (Bondaz *et al*, 2019). A fragment of APE-1 was amplified from cDNA and cloned into the final pDEST-
527 L4440 vector using Gateway technology (primer listed in Table S5). Double-stranded RNA (dsRNA)
528 for injections was produced with the Promega Ribomax RNA production system.

529 dsRNA was injected in L4/young adult hermaphrodites, which were then incubated at 20°C. For the co-
530 depletion of SDS-22 and GSP-1/-2, and co-depletion of GSP-1 and GSP-2, a mixture of 1:1 dsRNAs
531 was injected (Fig 4, Fig EV5, EV7). Embryos from injected worms were analyzed 16-20 hours after
532 injection.
533 RNA interference by feeding was performed on plates containing 1mM IPTG. The L4440 vector was
534 used as control. For the *pkc-3(ne4246)* strains and controls, worms were incubated on feeding plates at
535 semi-restrictive temperatures of 24°C (Fig 1, Fig 3D, Fig EV2A) or 22°C (Fig 3E,F,G). L4 larvae were
536 added to RNAi feeding plates and incubated for 24 hours. For co-depletion of SDS-22 and RPN-6.1/-7
537 (Fig 7, EV8-9), a mixture of 1:1 fresh bacteria culture was plated. Worms were incubated on feeding
538 plates at 20°C for 24h hours (Fig 5A, Fig 6A-E, Fig7, EV2B, EV3, EV8-9).
539
540 **Immunoprecipitation and mass spectrometry**
541 For immunoprecipitation experiments from embryos of mNeonGreen tagged GSP-2, worms were
542 grown in 3X PEP plates and embryos were harvested from gravid worms by bleaching (500 mM NaOH
543 and 5% bleach). The *N2* strain was used as a control. The mNeonGreen::GSP-2 and control
544 immunoprecipitations were performed in triplicate. Packed embryos were frozen in liquid nitrogen and
545 stored at −80°C. Embryos were then thawed, resuspended in immunoprecipitation buffer (100 mM KCl,
546 50 mM Tris (pH: 7.5), 1 mM MgCl2, 1 mM DTT, 5% glycerol, 0.2% NP-40, 1 mM EDTA, and protease
547 and phosphatase inhibitor cocktail (Roche)). The embryos were ground using a mill (Retsch MM301)
548 and silica beads (Lysing matrix C, MP Biomedicals). The protein homogenate was centrifuged at 14,000
549 rpm for 30 min at 4°C. The protein concentration in the supernatant was determined in a Bradford assay
550 (Bio-Rad Laboratories) using a UV/Vis Spectrophotomer (Labgene scientific). About 3 mg of
551 embryonic extract was incubated at 4°C for 1.5 h with 10 µl of mNeonGreen-Trap Agarose beads
552 (Chromotek), previously washed 3 times with IP buffer. After the incubation with the embryonic extract,
553 beads were washed three times with IP buffer, and three times with the buffer containing 100 mM KCl,
554 50 mM Tris (pH: 7.5), 1 mM MgCl2, 1 mM DTT, 1 mM EDTA to remove nonspecific binding. Elution
555 of mNeonGreen-tagged GSP-2 was performed by incubation of the beads for 10min at room
556 temperature with 25 µl of 0.15% TFA. The pH of the elution was corrected to pH: 7-8 with 0.5M Tris
557 (pH:7.9). 3 µl of the elutions were used to analyse the immunoprecipitation by western blot. 22 µl of
558 the elutions were snap frozen and sent to Biognosys (https://biognosys.com) for mass spectrometric
559 analysis. The elutions were subjected to denaturation, reduction, alkylation, digestion and C18 clean up.
560 The peptide digests were acquired in DIA mode using an Orbitrap Exploris 480 (Thermo Fisher) and
561 analyzed with directDIA (Spectronaut 15).
562
563 **Imaging of live embryos**
564 Adult hermaphrodites were dissected on a coverslip in a drop of Egg Buffer (118 mM NaCl, 48 mM
565 KCl, 2 mM $CaCl_2$, 2 mM $MgCl_2$, and 25 mM Hepes, pH 7.5). Embryos were mounted on a 3% agarose

566 pad for imaging. Time-lapse recordings, with frames captured every 10 seconds, were conducted using
567 a Nikon ECLIPSE Ni-U microscope equipped with a Nikon DS-U3 Digital Camera and a 60X/1.25
568 numerical aperture (NA) objective. Imaging was performed between 20 - 22°C.
569
570 **Immunostaining and imaging of fixed embryos**
571 Fixation and staining of embryos were carried out as described previously (Calvi *et al.*, 2022). The
572 primary antibody phospho-Histone 3 (Ser10) (Millipore, rabbit) was diluted 1:500 in PBST with 1%
573 BSA and slides incubated overnight at 4°C. Slides were then washed and incubated with the secondary
574 antibody (4 µg/ml Alexa Fluor 568–coupled anti-rabbit antibody) and 1 µg/ml DAPI to visualize DNA.
575 Images were acquired using a Nikon ECLIPSE Ni-U microscope, equipped with a Nikon DS-U3 Digital
576 Camera, and using a 60X/1.25 numerical aperture (NA) objective.
577
578 **Embryonic lethality**
579 To assess the embryonic lethality, young adult worms were singled on NGM plates seeded with OP50
580 and incubated at 20°C for 24 hours. Adults were the removed and the plates were incubated for an
581 additional 24 hours at 20°C (Fig 3C, Fig EV6, and other *sds-22(E153A)* mutants in *N2* and in *sds-*
582 *22::gfp* genetic backgrounds). The *mNG::gsp-2; sds-22(E153A)* strain was maintained as a *sds-*
583 *22(E153A)* heterozygote, since in the homozygote form it is 99.1% embryonic lethal. To quantify the
584 lethality of the homozygote, L4/young adult worms (homozygote wild-type, heterozygote, or
585 homozygote *sds-22(E153A)* mutant) were singled on OP50 seeded-NGM plates, allowed to lay eggs
586 for 24 hours, and subsequently lysed for genotyping. Homozygote *sds-22* wild-type and heterozygote
587 worms expressing wildtype *sds-22* from one allele and mutant *sds-22(E153A)* from the other allele were
588 used as a control. The embryonic lethality can be used to differentiate homozygotes from heterozygotes
589 and wild types for quantification (e.g. Fig 6F,G). However, since depletion of RNP-6.1 or RPN-7
590 resulted in few or no progeny (Fernando *et al.*, 2022), this precluded the possibility to analyze the
591 germlines of homozygote *mNG::gsp-2; sds-22(E153A)* worms with RNP-6.1 or RPN-7 depletion, as
592 we cannot distinguish the homozygote from the heterozygote.
593 SDS-22(E153A) mutation in wildtype *N2* exhibited 8.3% of lethality, while *sds-22(E153A)::gfp*
594 showed a lethality of 51.9%.
595
596 For the RNAi feeding and lethality assay of *pkc-3(ne4246)* mutant, L4 worms were initially transferred
597 to 1mM IPTG plates seeded with feeding bacteria and incubated overnight at 15°C. The following day,
598 young adult worms were singled onto feeding plate and incubated for 24 hours at 24°C (Fig 1A, 3D)
599 and 22°C (Fig 3E). After this period, the adult worms were removed and the plates were further
600 incubated at 24°C and 22°C respectively for 24 hours. The ratio of unhatched embryos to the total F1
601 progeny (unhatched embryos plus larvae) was used to calculate the percentage of embryonic lethality.
602

603 **Yeast two-hybrid assay**

604 The interaction between SDS-22 and GSP-1/-2 was assessed using a GAL4-based yeast two-hybrid
605 (Y2H) system (Gateway, Invitrogen) using the MAV203 yeast strain. Full-length SDS-22 (1-326)
606 fragments, both wild type and mutant (E153A), were fused to the GAL4 DNA binding domain (DBD,
607 Bait plasmid). Full-length cDNAs of GSP-1 and GSP-2 were fused to the GAL4 activation domain (AD,
608 Prey plasmid). The SDS-22 wild type and mutant fragments, GSP-1 and GSP-2 were first cloned into
609 the pDONR201, then transferred to the pDEST32 (GAL4DBD) and pDEST22 vector (GAL4AD)
610 separately using Gateway technology. Mutations were introduced by Pfu site-directed mutagenesis. A
611 list of plasmids and primers used for the Y2H assay is provided in Table S6 and S7 respectively.
612 Transformants were selected on synthetic defined (SD) medium lacking leucine and tryptophan.
613 Interactions were tested by spotting single colonies containing the desired plasmids on medium lacking
614 leucine, tryptophan and histidine, with 7.5mM of 3AT (3-amino-1,2,3- triazole, Sigma). Picture of the
615 plates were captured using the Fusion FX6 EDGE Imaging System (Vilber) equipped with an Evo-6
616 Scientific Grade CCD camera.

617

618 **Western blot**

619 Embryos obtained by hypochlorite treatment from two 5cm plates of adult worms were resuspended in
620 SDS sample buffer and denatured at 95°C for 5 minutes. Approximately 3000 embryos per sample were
621 loaded onto a 10% SDS-PAGE gel, followed by Western blotting with ECL detection (Vilber, Fusion
622 FX). Primary antibodies [(anti-TUBULIN (1/2500, mouse, Sigma), anti-mNeonGreen (1/1000, mouse,
623 ChromoTek) and anti-GFP (1/2500, rabbit, Pines)] were incubated overnight at 4°C. HRP-conjugated
624 secondary antibodies were incubated for 45 minutes at room temperature.

625 Band signal measurement for anti-TUBULIN, anti-mNeonGreen, and anti-GFP was performed in Fiji
626 ImageJ by drawing equal-sized ROIs over each band. Mean intensity values were used for
627 quantification, and background was subtracted using the mean intensity of an equivalent ROI placed
628 below the band of interest. The ratio of *ctrl(RNAi)* treatment was normalized to 1.

629

630 **Image analysis and measurement**

631 *Cortical PAR-2 intensity measurement (Fig1 B,C, Fig 3F,G)*

632 The line file of GFP::PAR-2 intensity along the entire cortex was measured in one-cell stage embryos
633 at pronuclear meeting. The stage of pronuclear meeting is defined when the two pronuclei first contact
634 each other. In *pkc-3(ne4246)* embryos, the two pronuclei exhibited a tendency to meet more centrally
635 compared to controls (Fig 1B, Movie EV1), as shown in (Kirby *et al*, 1990; Rodriguez *et al*, 2017).
636 Using ImageJ software, a free-line 5-pixel-wide was positioned at the anterior pole of the cortex
637 (position 0 µm) and traced manually along the whole cortex to the posterior pole (position 75 µm) and
638 back to the anterior pole. The background was subtracted from each value. The intensity of the line

639 profile (from 0 to 75 µm) of the segment traced was shown in an arbitrary unit (a.u.). Images were in
640 16-bit format.
641
642 *Cortical PAR-2 size measurement (Fig 1D, Fig 3B, Fig 4)*
643 The size of cortical GFP::PAR-2 domain was determined by measuring the length of the PAR-2 domain
644 normalized for the total perimeter of the embryo at pronuclear meeting. The perimeter of the embryo
645 and the length of the PAR-2 domain were measured by the Qupath software with machine learning, as
646 detailed previously (Vaudano *et al*, 2024). The length of the PAR-2 domain is represented as a
647 percentage of the total perimeter of the embryo.
648
649 *AB cell size measurement (Fig 1E,F)*
650 The total length of the embryo was measured manually from the anterior to the posterior pole using
651 ImageJ software. AB cell size was measured from the anterior pole to the cleavage midline when the
652 embryo just divided into two cells. The AB cell ratio was calculated as the proportion of AB cell size
653 relative to the total embryo length (AB cell plus P1 cell length).
654
655 *Protein intensity of mNG::GSP-2, GFP::GSP-1, SDS-22::GFP in embryos and germlines (Fig 6-7, Fig*
656 *EV4, Fig EV7-9)*
657 For embryos, the mean intensity of cytoplasmic mNG::GSP-2, GFP::GSP-1, SDS-22::GFP was
658 determined by tracing a fixed-length line in the cytoplasm from the anterior to the posterior of the
659 embryo (above the nucleus) at pronuclear meeting stage using the ImageJ software. The background
660 was subtracted from each value.
661 For the embryonic intensity of mNG::GSP-2 in the *sds-22(E153A)* mutant genetic background, which
662 is embryonic lethal, L4/young adult worms (homozygote wild type, heterozygote or homozygote
663 *mNG::GSP-2; sds-22(E153A)* mutant) were singled, let them lay few eggs, and subsequently dissected
664 for imaging. Homozygous *mNG::GSP-2; sds-22(E153A)* mutant worms were recognized by looking at
665 the progeny in the original plates, as homozygote *mNG::GSP-2; sds-22(E153A)* worms only lay dead
666 eggs. Homozygote *sds-22* wild-type and heterozygote worms expressing wildtype *sds-22* from one
667 allele and mutant *sds-22(E153A)* from the other allele were used as a control.
668 For germlines, mean cytoplasmic and nuclear intensities of mNG::GSP-2, GFP::GSP-1, SDS-22::GFP
669 were measured by drawing a fixed circle in the cytoplasm and/-or nucleus of -1 and -2 oocytes using
670 ImageJ. Background intensity was subtracted. The mean intensities of the cytoplasmic and nuclear
671 regions in -1 and -2 oocytes were calculated and reported.
672 The germline intensity of mNG::GSP-2 in the *sds-22(E153A)* mutant cannot be measured because there
673 were no viable embryos after depletion of RNP-6.1 or RNP-7, therefore the genotype of homozygous
674 *mNG::gsp-2; sds-22(E153A)* (also embryonic lethal) cannot be differentiated from the homozygote
675 wild type and heterozygote.

676
677 *Phospho-Histone 3 (Ser10) intensity measurement (Fig 5)*
678 One-cell stage embryos at anaphase were analyzed. A segment 5-pixel-wide and of constant length,
679 centered at the chromosomes was traced using ImageJ software. For each embryo, the average of three
680 segments (upper, center, and lower chromosomes) was used for quantification. The intensity of the line
681 profile of each embryo was normalized to the average of the value in the cytoplasm at position 0 of the
682 segment traced. The mean intensities of the phospho-Histone 3 (Ser10) on the chromosomes were
683 calculated and reported.
684
685 **Statistical analysis**
686 Statistical analysis was conducted using GraphPad Prism 9. Details on the statistical tests, sample sizes,
687 number of replicates, and interpretation of error bars are specified in each figure legend, within the
688 results section, or in the methods section, and summarized in Table S8. Data was assumed to have
689 normal distribution.
690 Significance was defined as: ns, $p > 0.05$, *$p < 0.05$, **$p < 0.01$, ***$p < 0.001$, ****$p < 0.0001$.
691
692
693
694 **Data availability**
695 All the strains and reagents generated in this study are available from the corresponding author upon
696 request. All raw data associated with the experiments will be deposited in Yareta at publication.
697
698 **Author Contributions**
699 Yi Li: Conceptualization; Formal analysis; Investigation; Visualization; Writing-original draft;
700 Writing-review and editing. Ida Calvi: Conceptualization; Investigation; Writing-review and editing.
701 Monica Gotta: Conceptualization; Funding acquisition; Supervision; Writing-original draft; Writing-
702 review and editing
703
704 **Funding**
705 This research was funded in part by the Swiss National Science Foundation (SNSF) (grant number
706 31003A_175850). For the purpose of Open Access, a CC BY public copyright licence is applied to any
707 Author Accepted Manuscript (AAM) version arising from this submission.
708
709 **Disclosure and competing interest statement**
710 The authors declare no competing or financial interests.
711
712 **Acknowledgments**

A special thanks to Erik Griffin, and Dhanya Cheerambathur for strains. We would like to thank all the present and past members of the Gotta, Meraldi and Steiner laboratories, Patrick Meraldi and Florian Steiner for discussions and suggestions. Thanks to Sofia Barbieri, Victoria von Glasenapp and Florian Steiner for comments on the manuscript. Some strains were provided by the CGC, which is funded by NIH Office of Research Infrastructure Programs (P40 OD010440). This research was funded by the Swiss National Science Foundation (grant number 31003A_175850) and the University of Geneva.

References

Aggen JB, Nairn AC, Chamberlin R (2000) Regulation of protein phosphatase-1. *Chem Biol* 7: R13-23

Ahringer J (2006) *Reverse Genetics. WormBook: The Online Review of C. elegans Biology [Internet]. WormBook; 2005-2018.*

Arribere JA, Bell RT, Fu BX, Artiles KL, Hartman PS, Fire AZ (2014) Efficient marker-free recovery of custom genetic modifications with CRISPR/Cas9 in Caenorhabditis elegans. *Genetics* 198: 837-846

Beacham GM, Wei DT, Beyrent E, Zhang Y, Zheng J, Camacho MMK, Florens L, Hollopeter G (2022) The Caenorhabditis elegans ASPP homolog APE-1 is a junctional protein phosphatase 1 modulator. *Genetics* 222

Billmyre KK, Doebley AL, Spichal M, Heestand B, Belicard T, Sato-Carlton A, Flibotte S, Simon M, Gnazzo M, Skop A *et al* (2019) The meiotic phosphatase GSP-2/PP1 promotes germline immortality and small RNA-mediated genome silencing. *PLoS Genet* 15: e1008004

Bondaz A, Cirillo L, Meraldi P, Gotta M (2019) Cell polarity-dependent centrosome separation in the C. elegans embryo. *J Cell Biol* 218: 4112-4126

Brenner S (1974) The genetics of Caenorhabditis elegans. *Genetics* 77: 71-94

Calvi I, Schwager F, Gotta M (2022) PP1 phosphatases control PAR-2 localization and polarity establishment in C. elegans embryos. *J Cell Biol* 221

Campanale JP, Sun TY, Montell DJ (2017) Development and dynamics of cell polarity at a glance. *J Cell Sci* 130: 1201-1207

Cao X, Lake M, Van der Hoeven G, Claes Z, Del Pino Garcia J, Lemaire S, Greiner EC, Karamanou S, Van Eynde A, Kettenbach AN *et al* (2024) SDS22 coordinates the assembly of holoenzymes from nascent protein phosphatase-1. *Nat Commun* 15: 5359

Cao X, Lemaire S, Bollen M (2022) Protein phosphatase 1: life-course regulation by SDS22 and Inhibitor-3. *FEBS J* 289: 3072-3085

Ceulemans H, Bollen M (2004) Functional diversity of protein phosphatase-1, a cellular economizer and reset button. *Physiol Rev* 84: 1-39

Ceulemans H, Vulsteke V, De Maeyer M, Tatchell K, Stalmans W, Bollen M (2002) Binding of the concave surface of the Sds22 superhelix to the alpha 4/alpha 5/alpha 6-triangle of protein phosphatase-1. *J Biol Chem* 277: 47331-47337

Cheng YL, Chen RH (2015) Assembly and quality control of the protein phosphatase 1 holoenzyme involves the Cdc48-Shp1 chaperone. *J Cell Sci* 128: 1180-1192

Choy MS, Moon TM, Ravindran R, Bray JA, Robinson LC, Archuleta TL, Shi W, Peti W, Tatchell K, Page R (2019) SDS22 selectively recognizes and traps metal-deficient inactive PP1. *Proc Natl Acad Sci U S A* 116: 20472-20481

Duan H, Wang C, Wang M, Gao X, Yan M, Akram S, Peng W, Zou H, Wang D, Zhou J *et al* (2016) Phosphorylation of PP1 Regulator Sds22 by PLK1 Ensures Accurate Chromosome Segregation. *J Biol Chem* 291: 21123-21136

761 Eiteneuer A, Seiler J, Weith M, Beullens M, Lesage B, Krenn V, Musacchio A, Bollen M,
762 Meyer H (2014) Inhibitor-3 ensures bipolar mitotic spindle attachment by limiting association
763 of SDS22 with kinetochore-bound protein phosphatase-1. *EMBO J* 33: 2704-2720
764 Fernando LM, Quesada-Candela C, Murray M, Ugoaru C, Yanowitz JL, Allen AK (2022)
765 Proteasomal subunit depletions differentially affect germline integrity in C. elegans. *Front Cell*
766 *Dev Biol* 10: 901320
767 Goehring NW (2014) PAR polarity: from complexity to design principles. *Exp Cell Res* 328:
768 258-266
769 Goldstein B, Macara IG (2007) The PAR proteins: fundamental players in animal cell
770 polarization. *Dev Cell* 13: 609-622
771 Grusche FA, Hidalgo C, Fletcher G, Sung HH, Sahai E, Thompson BJ (2009) Sds22, a PP1
772 phosphatase regulatory subunit, regulates epithelial cell polarity and shape [Sds22 in epithelial
773 morphology]. *BMC Dev Biol* 9: 14
774 Hao Y, Boyd L, Seydoux G (2006) Stabilization of cell polarity by the C. elegans RING protein
775 PAR-2. *Dev Cell* 10: 199-208
776 Hayer-Hartl M, Bracher A, Hartl FU (2016) The GroEL-GroES Chaperonin Machine: A Nano-
777 Cage for Protein Folding. *Trends Biochem Sci* 41: 62-76
778 Heroes E, Van der Hoeven G, Choy MS, Garcia JDP, Ferreira M, Nys M, Derua R, Beullens
779 M, Ulens C, Peti W *et al* (2019) Structure-Guided Exploration of SDS22 Interactions with
780 Protein Phosphatase PP1 and the Splicing Factor BCLAF1. *Structure* 27: 507-518 e505
781 Hsu JY, Sun ZW, Li X, Reuben M, Tatchell K, Bishop DK, Grushcow JM, Brame CJ, Caldwell
782 JA, Hunt DF *et al* (2000) Mitotic phosphorylation of histone H3 is governed by Ipl1/aurora
783 kinase and Glc7/PP1 phosphatase in budding yeast and nematodes. *Cell* 102: 279-291
784 Kamath RS, Fraser AG, Dong Y, Poulin G, Durbin R, Gotta M, Kanapin A, Le Bot N, Moreno
785 S, Sohrmann M *et al* (2003) Systematic functional analysis of the Caenorhabditis elegans
786 genome using RNAi. *Nature* 421: 231-237
787 Kapoor S, Kotak S (2019) Centrosome Aurora A regulates RhoGEF ECT-2 localisation and
788 ensures a single PAR-2 polarity axis in C. elegans embryos. *Development* 146
789 Kirby C, Kusch M, Kemphues K (1990) Mutations in the par genes of Caenorhabditis elegans
790 affect cytoplasmic reorganization during the first cell cycle. *Dev Biol* 142: 203-215
791 Klinkert K, Levernier N, Gross P, Gentili C, von Tobel L, Pierron M, Busso C, Herrman S,
792 Grill SW, Kruse K *et al* (2019) Aurora A depletion reveals centrosome-independent
793 polarization mechanism in Caenorhabditis elegans. *Elife* 8
794 Kubota H, Hynes G, Willison K (1995) The chaperonin containing t-complex polypeptide 1
795 (TCP-1). Multisubunit machinery assisting in protein folding and assembly in the eukaryotic
796 cytosol. *Eur J Biochem* 230: 3-16
797 Kueck AF, van den Boom J, Koska S, Ron D, Meyer H (2024) Alternating binding and p97-
798 mediated dissociation of SDS22 and I3 recycles active PP1 between holophosphatases. *Proc*
799 *Natl Acad Sci U S A* 121: e2408787121
800 Lang CF, Munro E (2017) The PAR proteins: from molecular circuits to dynamic self-
801 stabilizing cell polarity. *Development* 144: 3405-3416
802 Lesage B, Beullens M, Pedelini L, Garcia-Gimeno MA, Waelkens E, Sanz P, Bollen M (2007)
803 A complex of catalytically inactive protein phosphatase-1 sandwiched between Sds22 and
804 inhibitor-3. *Biochemistry* 46: 8909-8919
805 Llense F, Etienne-Manneville S (2015) Front-to-Rear Polarity in Migrating Cells. In: *Cell*
806 *Polarity 1: Biological Role and Basic Mechanisms*, Ebnet K. (ed.) pp. 115-146. Springer
807 International Publishing: Cham
808 Longhini KM, Glotzer M (2022) Aurora A and cortical flows promote polarization and
809 cytokinesis by inducing asymmetric ECT-2 accumulation. *Elife* 11

MacKelvie SH, Andrews PD, Stark MJ (1995) The Saccharomyces cerevisiae gene SDS22 encodes a potential regulator of the mitotic function of yeast type 1 protein phosphatase. *Mol Cell Biol* 15: 3777-3785

Meiselbach H, Sticht H, Enz R (2006) Structural analysis of the protein phosphatase 1 docking motif: molecular description of binding specificities identifies interacting proteins. *Chem Biol* 13: 49-59

Moreira S, Osswald M, Ventura G, Goncalves M, Sunkel CE, Morais-de-Sa E (2019) PP1-Mediated Dephosphorylation of Lgl Controls Apical-basal Polarity. *Cell Rep* 26: 293-301 e297

Motegi F, Zonies S, Hao Y, Cuenca AA, Griffin E, Seydoux G (2011) Microtubules induce self-organization of polarized PAR domains in Caenorhabditis elegans zygotes. *Nat Cell Biol* 13: 1361-1367

Moura M, Barbosa J, Pinto I, Leça N, Cunha-Silva S, Verza AE, Pedroso PD, Lemaire S, Duro J, Silva M *et al* (2024) POLO kinase inhibits Protein Phosphatase 1 to promote the Spindle Assembly Checkpoint and prevent aneuploidy. *bioRxiv*: 2024.2012.2023.630043

Munro E, Nance J, Priess JR (2004) Cortical flows powered by asymmetrical contraction transport PAR proteins to establish and maintain anterior-posterior polarity in the early C. elegans embryo. *Dev Cell* 7: 413-424

Ng K, Bland T, Hirani N, Goehring NW (2022) An analog sensitive allele permits rapid and reversible chemical inhibition of PKC-3 activity in C. elegans. *MicroPubl Biol* 2022

Papaevgeniou N, Chondrogianni N (2014) The ubiquitin proteasome system in Caenorhabditis elegans and its regulation. *Redox Biol* 2: 333-347

Pedelini L, Marquina M, Arino J, Casamayor A, Sanz L, Bollen M, Sanz P, Garcia-Gimeno MA (2007) YPI1 and SDS22 proteins regulate the nuclear localization and function of yeast type 1 phosphatase Glc7. *J Biol Chem* 282: 3282-3292

Peel N, Iyer J, Naik A, Dougherty MP, Decker M, O'Connell KF (2017) Protein Phosphatase 1 Down Regulates ZYG-1 Levels to Limit Centriole Duplication. *PLoS Genet* 13: e1006543

Peggie MW, MacKelvie SH, Bloecher A, Knatko EV, Tatchell K, Stark MJ (2002) Essential functions of Sds22p in chromosome stability and nuclear localization of PP1. *J Cell Sci* 115: 195-206

Peti W, Nairn AC, Page R (2013) Structural basis for protein phosphatase 1 regulation and specificity. *FEBS J* 280: 596-611

Posch M, Khoudoli GA, Swift S, King EM, Deluca JG, Swedlow JR (2010) Sds22 regulates aurora B activity and microtubule-kinetochore interactions at mitosis. *J Cell Biol* 191: 61-74

Qian J, Lesage B, Beullens M, Van Eynde A, Bollen M (2011) PP1/Repo-man dephosphorylates mitotic histone H3 at T3 and regulates chromosomal aurora B targeting. *Curr Biol* 21: 766-773

Riga A, Castiglioni VG, Boxem M (2020) New insights into apical-basal polarization in epithelia. *Curr Opin Cell Biol* 62: 1-8

Rodrigues NT, Lekomtsev S, Jananji S, Kriston-Vizi J, Hickson GR, Baum B (2015) Kinetochore-localized PP1-Sds22 couples chromosome segregation to polar relaxation. *Nature* 524: 489-492

Rodriguez J, Peglion F, Martin J, Hubatsch L, Reich J, Hirani N, Gubieda AG, Roffey J, Fernandes AR, St Johnston D *et al* (2017) aPKC Cycles between Functionally Distinct PAR Protein Assemblies to Drive Cell Polarity. *Dev Cell* 42: 400-415 e409

Santoro A, Vlachou T, Carminati M, Pelicci PG, Mapelli M (2016) Molecular mechanisms of asymmetric divisions in mammary stem cells. *EMBO Rep* 17: 1700-1720

Stone EM, Yamano H, Kinoshita N, Yanagida M (1993) Mitotic regulation of protein phosphatases by the fission yeast sds22 protein. *Curr Biol* 3: 13-26

858 Tzur YB, Egydio de Carvalho C, Nadarajan S, Van Bostelen I, Gu Y, Chu DS, Cheeseman IM,
859 Colaiacovo MP (2012) LAB-1 targets PP1 and restricts Aurora B kinase upon entrance into
860 meiosis to promote sister chromatid cohesion. *PLoS Biol* 10: e1001378
861 Vaudano AP, Schwager F, Gotta M, Barbieri S (2024) Internal feedback circuits among MEX-
862 5, MEX-6, and PLK-1 maintain faithful patterning in the Caenorhabditis elegans embryo. *Proc*
863 *Natl Acad Sci U S A* 121: e2407517121
864 Verbinnen I, Ferreira M, Bollen M (2017) Biogenesis and activity regulation of protein
865 phosphatase 1. *Biochem Soc Trans* 45: 89-99
866 Virshup DM, Shenolikar S (2009) From promiscuity to precision: protein phosphatases get a
867 makeover. *Mol Cell* 33: 537-545
868 Wurzenberger C, Held M, Lampson MA, Poser I, Hyman AA, Gerlich DW (2012) Sds22 and
869 Repo-Man stabilize chromosome segregation by counteracting Aurora B on anaphase
870 kinetochores. *J Cell Biol* 198: 173-183
871 Xin G, Fu J, Luo J, Deng Z, Jiang Q, Zhang C (2020) Aurora B regulates PP1gamma-Repo-
872 Man interactions to maintain the chromosome condensation state. *J Biol Chem* 295: 14780-
873 14788
874 Zhao P, Teng X, Tantirimudalige SN, Nishikawa M, Wohland T, Toyama Y, Motegi F (2019)
875 Aurora-A Breaks Symmetry in Contractile Actomyosin Networks Independently of Its Role in
876 Centrosome Maturation. *Dev Cell* 48: 631-645 e636
877

878

879 **Supplementary movies**

880 **Movie EV1: *sds-22(RNAi)* rescues PAR-2 posterior cortical localization in the *pkc-3(ne4246);***
881 ***gfp::par-2* embryos.**

882 *gfp::par-2* and *pkc-3*(*ne4246*); *gfp::par-2* embryos treated either with *ctrl*(*RNAi*) or *sds-22*(*RNAi*)
883 (RNAi by feeding). Acquisition of midplane fluorescent images begins during the early establishment
884 phase, and frames are captured every 10 s. In *gfp::par-2* embryos (both *ctrl*(*RNAi*) and *sds-22*(*RNAi*))
885 PAR-2 localizes at the posterior cortex in the one-cell stage embryo and in P1 in the two-cell stage
886 embryo (n = 12 for both). In *pkc-3*(*ne4246*); *gfp::par-2*, *ctrl*(*RNAi*) PAR-2 is uniformly distributed at
887 the cortex in both one- and two-cell stage embryo (n = 42). After depletion of SDS-22, *pkc-*
888 *3*(*ne4246*); *gfp::par-2* embryos showed PAR-2 posterior localization in one-cell stage embryo and in
889 the P1 cell (n = 42 out of 48). N = 5. n = number of embryos analyzed; N = number of independent
890 experiments. Anterior is to the left and posterior to the right. Referred to Fig 1B.

891

892 **Movie EV2: *sds-22*(*E153A*) substitution reduces the length of the PAR-2 cortical domain.**

893 Acquisition of midplane fluorescent images begins during the early stage, and frames are captured every
894 10 s. In *gfp::par-2; sds-22(E153A)* mutant embryos the length of cortical PAR-2 domain is decreased
895 compared to *gfp::par-2* embryos at pronuclear meeting stage (n = 30 and n = 52, respectively). N =
896 3. n = number of embryos analyzed. N = number of independent experiments. Anterior is to the left and
897 posterior to the right. Referred to Fig 3A,B.

898

Movie EV3: *sds-22*(*E153A*) substitution rescues PAR-2 posterior cortical localization in the *pkc-3*(*ne4246*); *gfp::par-2* embryos at 22°C.

Acquisition of midplane fluorescent images begins during the early stage, and frames are captured every 10 s. In *gfp::par-2; pkc-3*(*ne4246*); *sds-22(E153A)* mutant embryos PAR-2 is more enriched to the posterior cortex compared to *gfp::par-2; pkc-3*(*ne4246*) embryos where PAR-2 is localized all over the cortex (n = 19 for both genotypes). N = 3. n = number of embryos analyzed. N = number of independent experiments. Anterior is to the left and posterior to the right. Referred to Fig 3F,G.